Alumina–nano-nickel composite coatings on Al6061 substrate obtained by electrophoretic deposition

Hamoudi, Souaad; Bezzi, Nacer; Bensebaa, Farid; Delaporte, Philippe

Publisher's version / Version de l'éditeur:

https://doi.org/10.3390/jcs9030122

Journal of Composites Science, 9, 3, 2025-03-06

Journal of
Composites Science

MDPI

Article

Alumina–Nano-Nickel Composite Coatings on Al6061 Substrate Obtained by Electrophoretic Deposition

Souaad Hamoudi [1,*], Nacer Bezzi [1], Farid Bensebaa [2] and Philippe Delaporte [3]

[1] Technology Laboratory of Materials and Process Engineering (LTMGP), Faculty of Exact Sciences, University of Bejaia, Bejaia 06000, Algeria
[2] Energy, Mining and Environment Research Centre, National Research Council Canada, 1200 Montreal Road, Ottawa, ON K1A 0R6, Canada
[3] Aix-Marseille University, CNRS, Laboratory LP3 UMR 7341, Campus de Luminy, Case 917, CEDEX 09, 13288 Marseille, France
* Correspondence: souaad.hamoudi@univ-bejaia.dz

Abstract: Ceramic–nano-metallic composite coatings of Al_2O_3–nano-Ni on an aluminum substrate (Al6061) were obtained using electrophoretic deposition (EPD). Three composite coatings with different ratios of nano-Ni, i.e., 25, 50, and 75%, were obtained. The phase composition of the resulting composite coatings was examined using XRD; this confirmed the existence of alumina and nickel in the composite coatings. The surface morphology and microstructure of the composite coatings were analyzed with SEM, while the chemical composition and phase content were determined through energy-dispersive spectroscopy. The hardness indenter results revealed a high hardness 420 HV for the Ni 25% composite coating However the hardness decreased with an increase in the Ni nanoparticle ratio, reaching a value of 360 HV for the Ni 75% composite coating. Reflectance measurements were conducted using a UV–visible spectrophotometer equipped with an integrating sphere (UV2600), and the composite coating with a Ni ratio of 75% exhibited the lowest reflectance of UV–visible light at <0.035. These results are promising for subsequent investigations into the absorbance of Al_2O_3–nano-Ni composite coatings within the sunlight irradiation wavelength range.

Keywords: Al_2O_3–nano-Ni; composite coatings; electrophoretic deposition; microstructure; hardness; optical properties

Academic Editor: Jinyang Xu

Received: 5 January 2025
Revised: 24 February 2025
Accepted: 26 February 2025
Published: 6 March 2025

Citation: Hamoudi, S.; Bezzi, N.; Bensebaa, F.; Delaporte, P. Alumina–Nano-Nickel Composite Coatings on Al6061 Substrate Obtained by Electrophoretic Deposition. *J. Compos. Sci.* **2025**, *9*, 122. https://doi.org/10.3390/jcs9030122

1. Introduction

There is a strong focus on improving ceramic composites by incorporating nanoscale metallic particles [1]. These particles are commonly used to strengthen the ceramic matrix to produce materials with desirable properties [2], and they can be used in the power industry [3]. Al_2O_3 ceramics have seen widespread application due to their notable characteristics, including high hardness, excellent wear resistance, and elevated electrical resistivity [4]. Nickel is often chosen as a reinforcement due to its ability to maintain stability at high temperatures and due to its chemical inertness [2].

One of the most widely applied composite coatings is the Ni-Al_2O_3 system, which has good tribological [5,6], erosion and corrosion resistance [7,8], and wear and heat resistance [9,10] properties. It is widely used for many applications.

Ni-Al_2O_3 composite coatings also provide unique sets of surface characteristics, mainly such as selective surfaces for solar thermal conversion [11,12].

They are obtained using different methods, such as chemical methods [13], ultrasonic-assisted electrodeposition (UAED) [14], electrodeposition [15,16], planar magnetron-assisted RF sputtering [17], spin-coating [18], sol–gel [9], spark plasma sintering (SPS) [19], plasma spraying [20], planetary ball-milling [21], high-velocity flame spray (HVFS) systems [22], mechanochemical synthesis [4], cold-spraying coating [23], gel casting processes [1], centrifugal slip-casting method (CSC) [24], and electrophoretic deposition (EPD), which is utilized as a rapid prototyping method [25–28]. EPD is a colloidal process in which particles are compacted directly from a suspension under the effect of an electric field. This method offers several advantages, including the fabrication of films with thicknesses ranging from approximately ten nanometers to several hundred micrometers, simplicity, fast processing, cost-effectiveness, excellent uniformity, and the ability to work with substrates of any shape. It is widely used for the deposition of metal oxides for applications in various fields. Key advantages of EPD include its fast processing, cost-effectiveness, scalability, and the ability to achieve a broad range of compositions and thicknesses. EPD has already been widely adopted as an industrial process [29].

Some of the most common techniques, with their advantages and limitations, used to fabricate Ni-Al_2O_3 are summarized in Table 1.

Table 1. Most common methods used to prepare Ni-Al_2O_3 composite coatings.

Coating and Method	Advantages	Limitations
Nickel nano-particles embedded in a dielectric matrix of alumina. Spin-coating.	Uniform thin films. High reproducibility. Simple and fast process. Cost-effective for small-scale production. Good control over film thickness. Applicable to various materials.	Material waste. Limited to flat and small substrates. Solvent evaporation effects. Scalability issues [18].
Ni-Al_2O_3 composite film. Magnetron sputtering.	Dense and adherent coatings, high purity, fine microstructure. High control over thickness and composition. Used in microelectronics.	Expensive equipment. Requires vacuum environment and high-cost equipment. Low deposition rate [30,31].
Nano-structured Ni-Al_2O_3 composite coatings. Planetary ball-milling.	Versatile applications. Customizable parameters. Batch processing. Controllable atmosphere.	High wear and contamination. High energy consumption. Small batch processing. Agglomeration of fine powders [32].
Nickel–alumina composite coatings. Thermal spraying.	High deposition rates, suitable for large surfaces. Allows for thick coatings with good wear resistance and high hardness.	Requires expensive equipment. Some processes induce thermal stress, affecting adhesion [22,33].
Nickel–alumina composite coatings. Cold-spraying.		
Ni-Al_2O_3 nano composite coating. Electrodeposition.	Good adhesion, cost-effective, scalable for industrial applications.	Particle dispersion in the electrolyte can be challenging, possible agglomeration. Requires optimization of bath composition and deposition parameters, need many chemicals [19,34].
Electrophoretic deposition (EPD), used in our study.	Uniform coating, precise control over composition, simple setup, and suitable for complex shapes. Eco friendly process.	Adhesion strength depends on substrate preparation [28].

The present work aimed to use the electrophoretic deposition method to obtain metal–ceramic Al_2O_3–nano-Ni composite coatings with good properties using a colloidal suspension containing both metallic Ni nanoparticles and ceramic sub-micron Al_2O_3 particles with different ratios (Ni ratios: 25, 50, and 75%).

The choice of Al6061 as the substrate is crucial due to its excellent mechanical strength, corrosion resistance, and thermal conductivity, making it ideal for functional coatings. These properties ensure the longevity and effectiveness of the coating. Al6061's surface morphology, which may require pre-treatment for optimal roughness, affects the adhesion strength, while its surface energy and oxide layer influence the coating's uniformity and durability. Overall, Al6061 not only offers practical advantages but also significantly impacts the deposition process, ensuring the desired performance and durability of the coating [16,35].

The coatings obtained have the potential to be applied as selective absorbers.

2. Methods and Materials

2.1. Experiments

Alumina powder and aluminium substrate (Al6061) were sourced from Alfa-Aesar (Ward Hill, MA, USA), while nickel nanopowder was supplied by Vale-Inco (Toronto, ON, Canada). The alumina powder had an average particle size of approximately 400 nm, and the nickel powder had an average particle size of about 50 nm. Pure ethanol, ammonium hydroxide, and hydrochloric acid were procured from Sigma Aldrich.

The aluminium (Al6061) substrates had a rectangular shape measuring 30 × 10 mm^2. First, the substrates were polished using silicon carbide papers (400, 600, 1000, and 1200 grit) and then cleaned by sonication in ethanol followed by acetone for 5 min to eliminate surface residues, and they were finally dried at room temperature.

Nano-nickel and alumina powders were separately dispersed in pure ethanol solvent, where a suspension concentration of 1 mol% was used, and the mixtures were sonicated over 24 h. Extended sonication was necessary in order to achieve higher-quality films. Once dispersed, these two solutions were mixed at different mass ratios of nickel nanoparticles in the mixture ($Ni_{25\%}$, $Ni_{50\%}$, and $Ni_{75\%}$) and kept under stirring for 30 min. The pH of the single and mixed suspensions was adjusted to a range between 4.5 and 5 by adding HCl to lower it (acidic) and NH_4OH to raise it (basic).

Electrophoretic deposition (EPD) was performed using two aluminum electrodes with a 10 mm distance between them. The electrophoretic deposition was carried out under constant stirring at 100 rpm with an applied voltage of 10 V for a maximum of 30 min. Figure 1 provides a schematic representation of the experimental process.

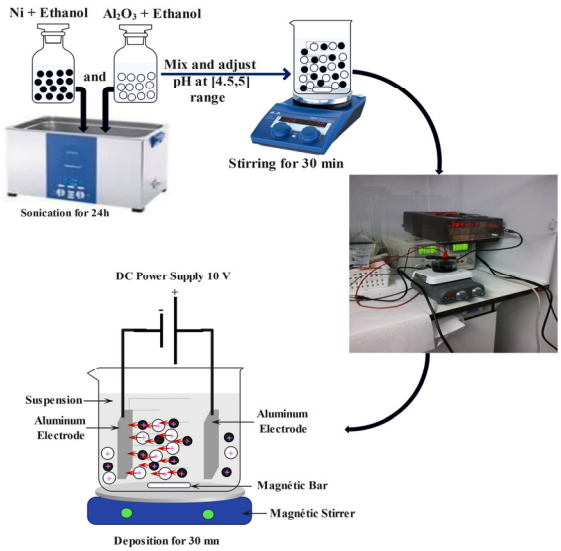

Figure 1. Schematic illustration of the experiment process.

2.2. Characterization

A MALVERN ZETASIZER was used to control the zeta potential of the mixtures (Ni + ethanol, Al_2O_3 + ethanol, and Ni + Al_2O_3 + ethanol) before the electrophoretic deposition process to confirm the stability of the charged particles.

The zeta potentials of each mixture (Ni + ethanol, Al_2O_3 + ethanol, and Ni + Al_2O_3 + ethanol) were measured at pH = 4.5. Their values were around 23, 50, and 41 mV, respectively, which was suitable for ensuring good coatings because of the particles' stability in the suspension [36].

A Veeco Dektak 150 Surface Profiler was used to measure the thickness of the composite coatings.

X-ray diffraction was used to identify the phases present in the composite coatings. The measurements were performed using a RIGAKU MINIFLEX X-ray diffractometer with a Cu Kα radiation source (λ = 1.5418 Å). Scans were conducted from 2θ = 10–80° at a rate of 0.01° min^{-1}.

Scanning electron microscopy (SEM) images were obtained for the composite coatings with an FEI CONTA 200 electron microscope equipped with an energy-dispersive X-ray analysis device (EDS analysis).

In terms of UV–visible spectrometry, optical spectra were recorded using a (UV2600 SHIMADZU, Kyoto, Japan) UV–visible spectrophotometer with an expanded wavelength range of up to 1400 nm equipped with an integrated sphere.

The Vickers hardness of the composite coatings was measured using an INNOVATEST hardness tester. The composite coatings were indented with a pyramidal diamond indenter under a 100 g load and 10 s time duration. Each coating was tested five times, and the average of these measurements was reported as the final Vickers hardness value for the tested coating.

3. Discussion and Results

The thicknesses of all the composite coatings were measured by mechanical surface profiling.

The effect of the duration time on the thicknesses of the obtained composite coatings under electrophoretic deposition was investigated, and the results are shown in Figure 2.

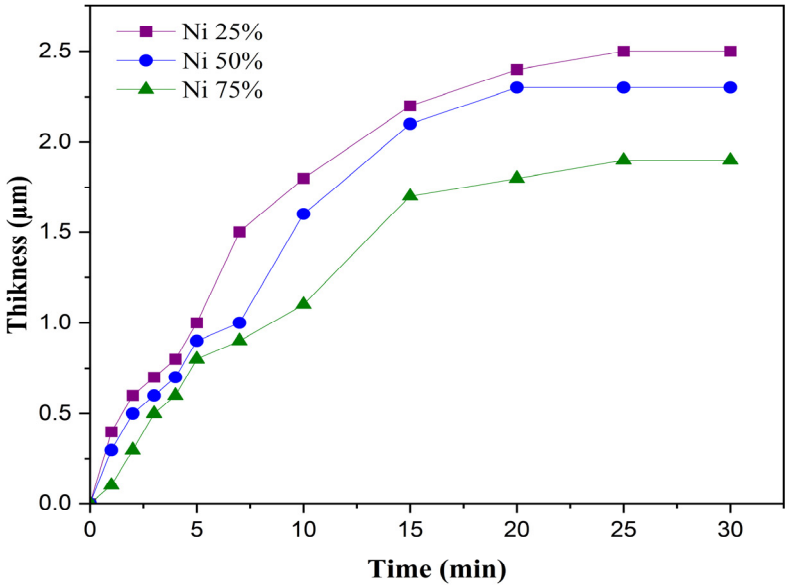

Figure 2. Effect of the time duration on the thicknesses of Al_2O_3–nano-Ni composite coatings at different ratios of nano- Ni: 25, 50, 75%.

Figure 2 shows that for the three composite coatings ($Ni_{25\%}$, $Ni_{50\%}$, and $Ni_{75\%}$) obtained, as the deposition time increased, the thickness of the coating also increased. In the initial stage (0 to 15 min) of EPD, the coating thickness increased almost linearly with the deposition time. This was because more charged particles were migrating toward the electrode and accumulating on the surface.

As the time progressed (15 to 20 min), the growth rate slowed down due to the following:

- Increased resistance: A thicker deposited layer increased the electrical resistance, reducing particle mobility.
- Electrostatic repulsion: A high charge density in the coating may have led to repulsion between incoming particles.
- Limited particle availability: The concentration of suspended particles in the bath decreased over time.

The thickness values were about 2.5, 2.3, and 2 µm for $Ni_{25\%}$, $Ni_{50\%}$, and $Ni_{75\%}$ at a 30 min duration, respectively. The thicknesses of the thin films increased with the increase in the alumina percentage; this can be explained by the fact that the particle size of the alumina was larger than that of the nickel used.

The X-ray spectra of composite coatings with different ratios of Ni: Al_2O_3 during the co-deposition are delineated in Figure 3.

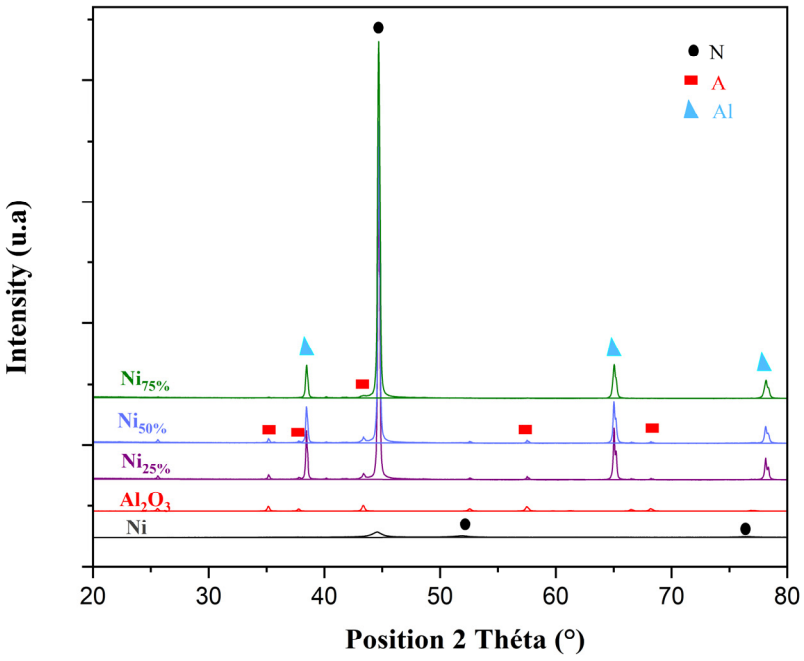

Figure 3. X-ray diffraction patterns of Al_2O_3, Ni nanoparticles, and Ni-Al_2O_3 composite coatings at different ratios of Ni. (N: nickel; A: alumina; Al: aluminium).

The XRD data were processed using the X'Pert HighScore software v5.3, and the ICDD Powder Diffraction database was employed for phase matching.

The results revealed the formation of the Al_2O_3–nano-Ni composite coatings on the aluminium substrate Al6061. The diffraction peaks of the Ni-Al_2O_3 composite coatings at 2θ values of 44.37°, 51.59°, and 76.1° corresponded to the preferred cubic Ni planes (111), (200), and (220), respectively (ICDD ref. card: 00-001-1258). The peaks attributed to rhombohedral alumina were detected at 2θ values of around 35.16°, 37.93°, 43.47°, 52.55°, 57.95°, and 68.42°, corresponding to the (104), (110), (113), (024), (116), and (300) crystal planes, respectively (ICDD ref. card: 00-001-1243). The peaks corresponding to cubic

aluminum were detected at 2θ values of 38.49° and 78.22° (ICDD ref. card: 98-004-4321). These peaks were related to the substrate used [37–39].

As shown in Figure 3, the intensity of the peak corresponding to Ni increased with the increase in the Ni ratio. In the metal-rich sample ($Ni_{75\%}$), we observed a high relative intensity of the (111) plane, which was attributed to the preferred growth of Ni nanoparticles. Ni-Al_2O_3 composites have also demonstrated comparable outcomes in earlier studies [40,41].

SEM micrographs of the Ni-Al_2O_3 composite coatings with different ratios of Ni (Ni ratio: 25, 50, and 75%) are shown in Figure 4.

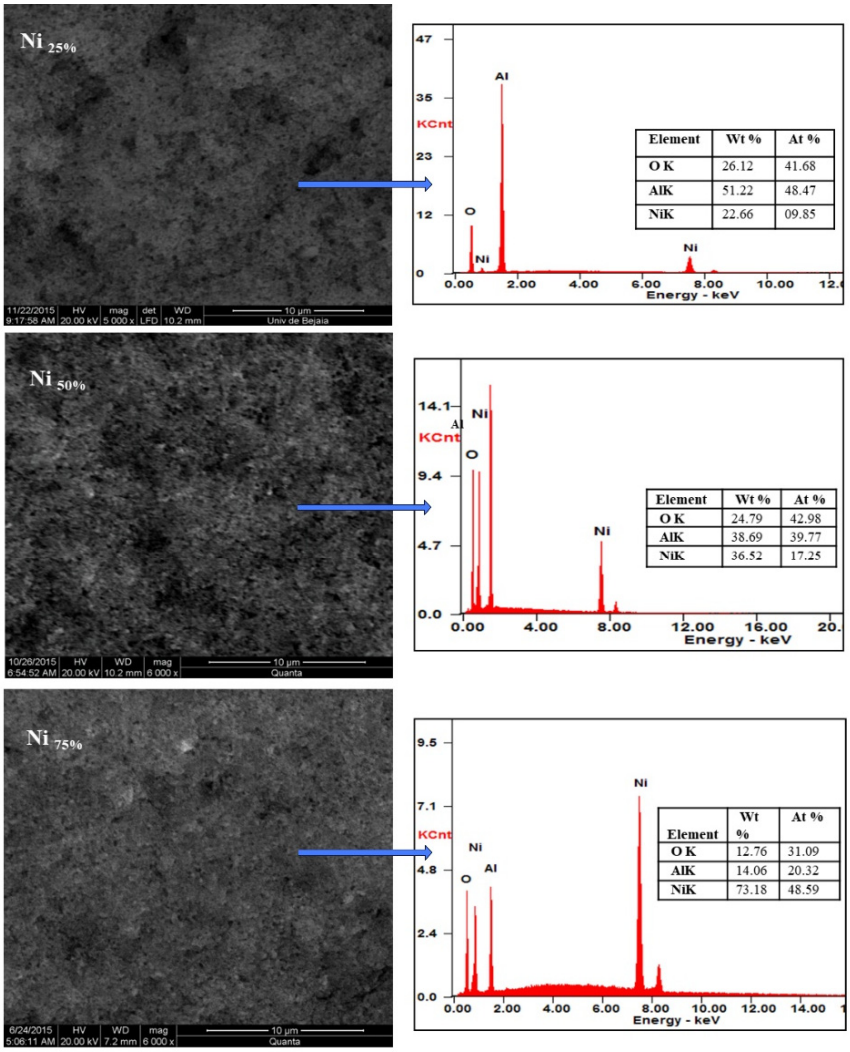

Figure 4. SEM micrographs and EDS spectra of Al_2O_3–nano-Ni composite coatings at different nano-Ni ratios.

The morphology and composition of the Ni-Al_2O_3 composite coatings were analyzed to evaluate the ability to control the deposition across the full range of mixture compositions. Typical micrographs of the composite coatings at different Ni contents are presented in Figure 3, they exhibited a relatively homogeneous structure, with a uniform distribution of Ni nanoparticles in the Ni-Al_2O_3 composite coatings, and there was no sign of agglomeration. They revealed a more strengthened structure with the increase in the metal nanoparticle content ($Ni_{75\%}$).

According to the EDS analysis results reported in Figure 3, there was a difference between the composition measured by EDS and the theoretical composition; this can be ex-

plained by the difference in the particle size of the two powders used in the electrophoretic deposition onto the surface. Consequently, the smaller nickel nanoparticles were deposited first, followed by the larger alumina particles. Indeed, the deposition kinetics of the larger particles (alumina) were expected to be relatively slower [42].

The EPD process produced composite coatings with a more homogeneous structure, ensuring better dispersion of Al_2O_3 and nano-Ni in the coatings.

The hardness of the composite coatings as a function of the Ni particle content in the mixture is plotted in Figure 5.

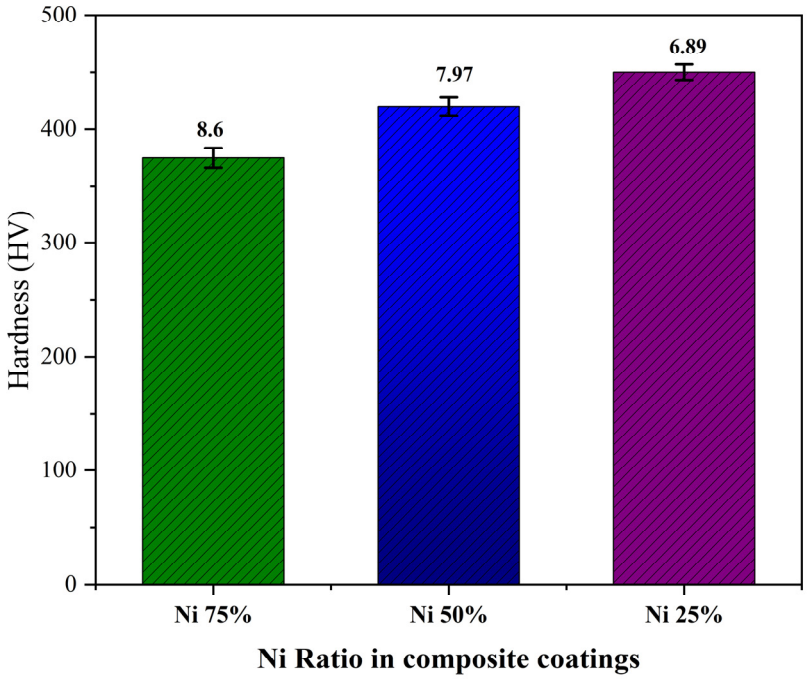

Figure 5. Vickers hardness (HV) and error bars of the standard deviation of the Al_2O_3–nano-Ni composite coatings at different ratios of nanometallic Ni: 25, 50 A 75%.

The standard deviation values were <10, indicating moderate variability in the measurements. This means that the data points were relatively close to the mean, suggesting a reasonable level of consistency and precision in the measurements.

It can be seen that the hardness of the Al_2O_3–nano-Ni composite coatings increased with the increase in the Al_2O_3 content from 375 HV for the rich-nickel ($Ni_{75\%}$) to 450 HV for the poor-nickel ($Ni_{25\%}$) composite.

Thus, the hardness of the Ni-Al_2O_3 composite coatings increased with the increase in the ceramic Al_2O_3 content.

Figure 6 shows a schematic diagram illustrating the strengthening mechanism of the supplementary hardness in the Al_2O_3–nano-Ni composite coatings on the AL6061 substrate, providing a clear visualization of these effects.

This can be explained by the intrinsic hardness of Al_2O_3 and its ability to reinforce the composite structure through the load transfer effect. Al_2O_3 acts as a load-bearing reinforcement, enhancing the composite's hardness and making the coating more resistant to deformation, thereby increasing its overall hardness. This inclusion aligns with previous studies and reinforces the results obtained [9,21,43–48].

As shown in Figure 6, the EPD-produced Al_2O_3–nano-Ni composite coatings exhibited improved hardness due to the homogenous distribution of the Al_2O_3 and nano-Ni particles. This uniform dispersion effectively hindered dislocation movement, enhancing the coating's hardness through dispersion strengthening. Conversely, the electrodeposited

Al_2O_3-nano-Ni coatings also demonstrated increased hardness; however, ensuring a consistent nanoparticle distribution is challenging, which may result in agglomeration and reduced reinforcement efficiency [37].

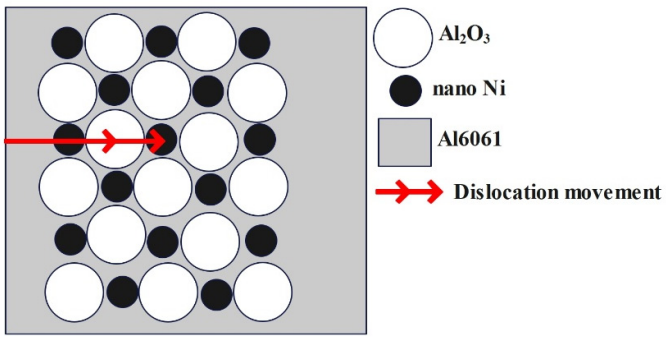

Figure 6. Schematic diagram of hardness enhancement in Al_2O_3–nano-Ni composite coatings.

As shown in Table 2, the hardness reproducibility values for each composite coating in the second and third trials exceeded 97%, indicating minimal differences between their means and demonstrating high measurement consistency and reliability.

Table 2. Results of reproducibility percentage and stability percentage of the second and third trials for hardness values obtained for Al_2O_3–nano-Ni composite coatings at different ratios of nanometallic Ni: 25, 50, and 75%.

Trial	Mean Hardness (HV)	Standard Deviation	Reproducibility (%)	Stability (%)
$Ni_{25\%}$ 1st	375	6.89	-	-
$Ni_{25\%}$ 2nd	364	6.5	97.07	94.34
$Ni_{25\%}$ 3rd	371	6.08	98.08	93.54
$Ni_{50\%}$ 1st	420	7.96	-	-
$Ni_{50\%}$ 2nd	418	7.38	99.5	92.71
$Ni_{50\%}$ 3rd	424	6.78	98.56	91.87
$Ni_{75\%}$ 1st	450	8.6	-	-
$Ni_{75\%}$ 2nd	445	7.18	98.89	83.49
$Ni_{75\%}$ 3rd	455	6.81	97.75	94.85

The stability percentages for the Al_2O_3–nano-Ni composite coatings (Ni ratio: 25% and 50%) were >91%, signifying low variation within each trial and stable results.

For the Al_2O_3–nano-Ni composite coating with 75% Ni, the stability increased from 83% to 94%, suggesting improved precision and control in the third trial. This increase reflects enhancements in the quality of the method, addressing issues such as calibration errors, measurement inconsistencies, or procedural variations observed in the second trial, leading to a more stable process. These results imply that the electrophoretic deposition method is reliable.

The resulting reflectance spectra of the composite coatings at the different Ni ratios are given in Figure 7.

The reflectance spectra of the Al_2O_3–nano-Ni composite coatings with different Ni contents exhibited lower reflectance values with the increase in the nano NI content, as shown in Figure 7. The coating with a 75% of nano Ni content revealed the lowest reflectance in visible light of <0.035; while the composite coating with higher nickel nanoparticle content absorbed light significantly. This makes it suitable for selective absorbers due to its adjustable optical properties. Composite films strongly absorb visible light due to two key physical phenomena: the first is due to inter-band transitions in the metal; as nickel

is a transition metal, it has electronic states that allow for these transitions, leading to strong absorption and small particle resonance or plasmonic effects; nickel nanoparticles contribute to plasmonic resonance, a phenomenon where light interacts with small metallic particles, causing enhanced absorption. This effect is more pronounced when the Ni content is high, further reducing the reflectance [49,50].

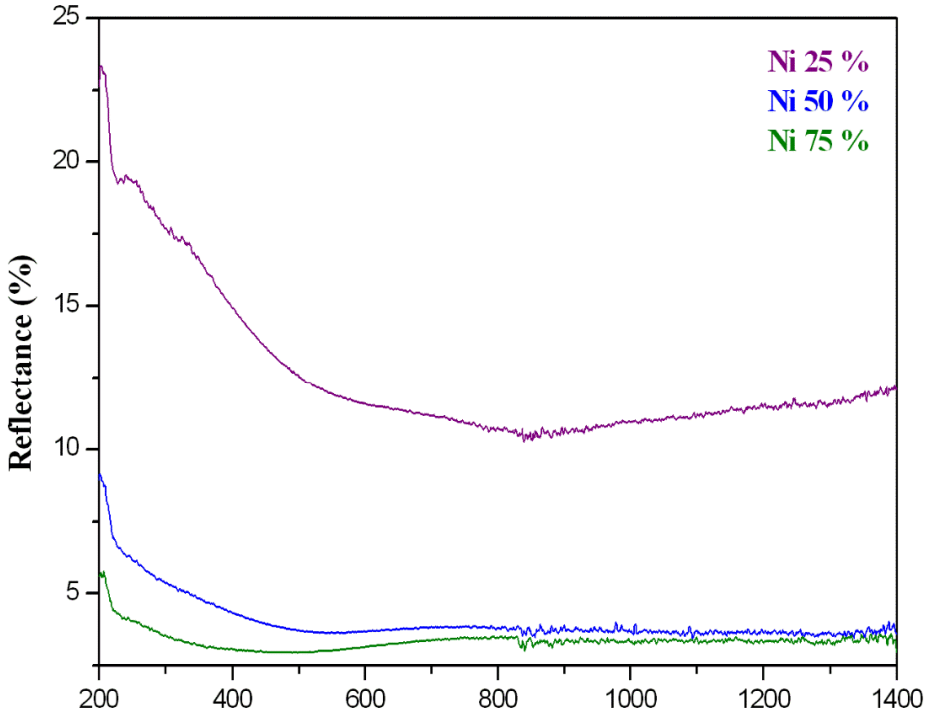

Figure 7. Reflectance UV–visible spectra of Al_2O_3–nano-Ni composite coatings at different ratios of nanometallic Ni: 25, 50, and 75%.

4. Conclusions

Composite coatings with sub-micron alumina and nanometallic nickel particles were successfully deposited on Al6061 substrate using EPD techniques with varying ratios of Ni metallic nanoparticles of 25, 50, and 75% in the colloidal mixture.

The XRD analysis demonstrated improved alumina and nickel peaks in the composite coatings.

The SEM micrographs exhibited regular surfaces for the composite coatings, with more uniformity in the $Ni_{75\%}$ composite coating.

The EDS analysis revealed that the nanometallic nickel and alumina particles had content ratios proportional to the initial mixture conditions.

The $Ni_{25\%}$ composite coating showed the highest microhardness, averaging 450 HV. When the alumina content was reduced, the microhardness decreases, with it being the lowest for the $Ni_{75\%}$ coating, with an average hardness of 375 HV. However, the difference was not very significant.

The reproducibility and stability percentages of the hardness results obtained for Al_2O_3–nano-Ni composite coatings, along with the results from the second and third trials, imply that the electrophoretic deposition method is reliable.

The optical behaviour of the Al_2O_3–nano-Ni composite coatings with the variation in the Ni content was studied, and the results showed an improved low reflectance (<0.035). The Ni nanoparticle content in the coatings was the first cause of selectivity. The presented results showing improvements in the composite's adjustable optical properties are promising for subsequent investigations and make it suitable for selective absorber applications.

Author Contributions: Conceptualization, S.H.; methodology, S.H. and F.B.; investigation, S.H., N.B. and P.D.; writing—original draft preparation, S.H.; writing—review and editing, S.H.; supervision, N.B. All authors have read and agreed to the published version of the manuscript.

Funding: This research received no external funding.

Data Availability Statement: The original contributions presented in this study are included in the article. Further inquiries can be directed to the corresponding author.

Conflicts of Interest: The authors declare no conflicts of interest.

References

1. Niihara, K.; Kim, B.S.; Nakayama, T.; Kusunose, T.; Nomoto, T.; Hikasa, A.; Sekino, T. Fabrication of Complex-Shaped Alumina/Nickel Nanocomposites by Gelcasting Process. *J. Eur. Ceram. Soc.* **2004**, *24*, 3419–3425. [CrossRef]
2. Lee, S.J.; Chun, S.Y.; Lee, C.H.; Yoon, Y.S. Fabrication of Nanosized Alumina Powders by a Simple Polymer Solution Route. *J. Nanosci. Nanotechnol.* **2006**, *6*, 3633–3636. [CrossRef] [PubMed]
3. Shchegolkov, A.V.; Lipkin, M.S.; Shchegolkov, A.V. Preparation of WO_3 Films on Titanium and Graphite Foil for Fuel Cell and Supercapacitor Applications by Electrochemical (Cathodic) Deposition Method. *Russ. J. Gen. Chem.* **2022**, *92*, 1161–1167. [CrossRef]
4. Xu, S.; Zhao, M.; Cai, Z.; Sun, N.; Liu, F.; Du, B.; Zhang, X.; Ling, Z. Effect of Annealing on the Microwave-Absorption Properties of Ni/Al_2O_3 Nanocomposites. *Acta Metall. Sin.* **2013**, *26*, 385–389. [CrossRef]
5. Karthik, R.; Mani, R.; Manikandan, P. Tribological Studies of Ni-SiC and Ni-Al_2O_3 Composite Coatings by Pulsed Electrodeposition. *Mater. Today Proc.* **2020**, *37*, 701–706. [CrossRef]
6. Singh, A.; Kumar, H.; Kumar, S. Tribological Performance of Thermally Sprayed Ni-Cr_2O_3 and Ni-Al_2O_3 coatings on Pipeline Steel Using Taguchi's Approach. *Mater. Today Proc.* **2020**, *41*, 976–981. [CrossRef]
7. Sun, Y.; Flis-Kabulska, I.; Flis, J. Corrosion Behaviour of Sediment Electro-Codeposited Ni-Al_2O_3 Composite Coatings. *Mater. Chem. Phys.* **2014**, *145*, 476–483. [CrossRef]
8. Noorbakhsh Nezhad, A.H.; Mohammadi Zahrani, E.; Alfantazi, A.M. Erosion-Corrosion of Electrodeposited Superhydrophobic Ni-Al_2O_3 Nanocomposite Coatings under Jet Saline-Sand Slurry Impingement. *Corros. Sci.* **2022**, *197*, 110095. [CrossRef]
9. Yetim, T.; Turalioğlu, K.; Taftali, M.; Tekdir, H.; Kovaci, H.; Yetim, A.F. Synthesis and Characterization of Wear and Corrosion Resistant Ni-Doped Al_2O_3 Nanocomposite Ceramic Coatings by Sol-Gel Method. *Surf. Coatings Technol.* **2022**, *444*, 128659. [CrossRef]
10. Chen, J. Characteristic Of Ni-Al_2O_3 Nanocomposition Coatings. *Procedia Eng.* **2011**, *15*, 4414–4418. [CrossRef]
11. Banthuek, S.; Suriwong, T.; Nunocha, P.; Andemeskel, A. Application of Ni-Al_2O_3 Cermet Coating on Aluminium Fin as the Solar Absorber in Evacuated Tube Collector (ETC). *Mater. Today Proc.* **2018**, *5*, 14793–14798. [CrossRef]
12. Chevapruk, T.; Chomcharoen, N.; Techapiesancharoenkij, R.; Kumnorkaew, P.; Muangnapoh, T.; Surawathanawises, K. Solution-Based Ni-Al_2O_3 Solar Selective Coating Using Convective Deposition. *Mater. Today Proc.* **2020**, *23*, 745–751. [CrossRef]
13. Li, G.J.; Huang, X.X.; Guo, J.K. Fabrication, Microstructure and Mechanical Properties of Al 2O3/Ni Nanocomposites by a Chemical Method. *Mater. Res. Bull.* **2003**, *38*, 1591–1600. [CrossRef]
14. Ma, C.Y.; Zhao, D.Q.; Xia, F.F.; Xia, H.; Williams, T.; Xing, H.Y. Ultrasonic-Assisted Electrodeposition of Ni-Al_2O_3 Nanocomposites at Various Ultrasonic Powers. *Ceram. Int.* **2020**, *46*, 6115–6123. [CrossRef]
15. Pradeep, D.G.; Sharath, B.N.; Afzal, A.; Ahmed Ali Baig, M.; Shanmugasundaram, M. Study on Scratch Behavior of Ni-Al_2O_3 coating Composition on Al-2219 Substrate by Electro Deposited Technique. *Mater. Today Proc.* **2021**, *46*, 8716–8722. [CrossRef]
16. Raghavendra, C.R.; Basavarajappa, S.; Sogalad, I.; Mathad, S. Comparative Study on Ni and Ni-α-Al_2O_3Nano Composite Coating on Al6061 Substrate Material. *Mater. Today Proc.* **2020**, *24*, 975–982. [CrossRef]
17. Sathiaraj, S.; Thangaraj, R.; Agnihotri, P. High Absorptance and Low Emittance AR-Coated Ni-Al_2O_3 Solar Absorbers. *J. Phys. D Appl. Phys.* **1990**, *23*, 250. [CrossRef]
18. Boström, T.; Wäckelgård, E.; Westin, G. Solution-Chemical Derived Nickel-Alumina Coatings for Thermal Solar Absorbers. *Sol. Energy* **2003**, *74*, 497–503. [CrossRef]
19. Feng, T.; Zheng, W.; Chen, W.; Shi, Y.; Fu, Y.Q. Enhanced Interfacial Wettability and Mechanical Properties of Ni@Al2O3/Cu Ceramic Matrix Composites Using Spark Plasma Sintering of Ni Coated Al_2O_3 Powders. *Vacuum* **2021**, *184*, 109938. [CrossRef]
20. Valette, S.; Bernardie, R.; Absi, J.; Lefort, P. Elaboration and Characterisation of Plasma Sprayed Alumina Coatings on Nickel with Nickel Oxide Interlayer. *Surf. Coatings Technol.* **2021**, *416*, 127159. [CrossRef]
21. Yazdani, A.; Isfahani, T. Hardness, Wear Resistance and Bonding Strength of Nano Structured Functionally Graded Ni-Al_2O_3 Composite Coatings Fabricated by Ball Milling Method. *Adv. Powder Technol.* **2018**, *29*, 1306–1316. [CrossRef]

22. Grewal, H.S.; Singh, H.; Agrawal, A. Microstructural and Mechanical Characterization of Thermal Sprayed Nickel-Alumina Composite Coatings. *Surf. Coatings Technol.* **2013**, *216*, 78–92. [CrossRef]
23. Sevillano, F.; Poza, P.; Múnez, C.J.; Vezzù, S.; Rech, S.; Trentin, A. Cold-Sprayed Ni-Al2O3 Coatings for Applications in Power Generation Industry. *J. Therm. Spray Technol.* **2013**, *22*, 772–782. [CrossRef]
24. Zygmuntowicz, J.; Wachowski, M.; Miazga, A.; Konopka, K.; Kaszuwara, W. Characterization of Al_2O_3/Ni Composites Manufactured via CSC Technique in Magnetic Field. *Compos. Part B Eng.* **2019**, *156*, 113–120. [CrossRef]
25. Ferrari, B.; Sánchez-Herencia, A.J.; Moreno, R. Nickel-Alumina Graded Coatings Obtained by Dipping and EPD on Nickel Substrates. *J. Eur. Ceram. Soc.* **2006**, *26*, 2205–2212. [CrossRef]
26. Babadi, P.; Sadreddini, S.; Mohsenifar, F.; Roshani, M. The Influence of Electrophoretic Potential on Ni—Al_2O_3 Nano-Composite Coating. *Prot. Met. Phys. Chem. Surf.* **2016**, *52*, 249–253. [CrossRef]
27. Pikalova, E.Y.; Kalinina, E.G. Electrophoretic Deposition in the Solid Oxide Fuel Cell Technology: Fundamentals and Recent Advances. *Renew. Sustain. Energy Rev.* **2019**, *116*, 109440. [CrossRef]
28. Corni, I.; Ryan, M.P.; Boccaccini, A.R. Electrophoretic Deposition: From Traditional Ceramics to Nanotechnology. *J. Eur. Ceram. Soc.* **2008**, *28*, 1353–1367. [CrossRef]
29. Hu, S.; Li, W.; Finklea, H.; Liu, X. A Review of Electrophoretic Deposition of Metal Oxides and Its Application in Solid Oxide Fuel Cells. *Adv. Colloid Interface Sci.* **2020**, *276*, 102102. [CrossRef]
30. Rezaei, R.; Moradi, G. Study of the Performance of Dry Methane Reforming in a Microchannel Reactor Using Sputtered Ni/Al2O3 Coating on Stainless Steel. *Int. J. Hydrogen Energy* **2018**, *43*, 21374–21385. [CrossRef]
31. Stephen, T.; Thangaraj, R.; Sharbaty, H.A.L.; Agnihotri, P. Optical properties of selectively absorbing r.f. sputtered Ni-Al2O3 composite films. *Thin Solid Films* **1991**, *195*, 33–42. [CrossRef]
32. Yazdani, A.; Isfahani, T. A Facile Method for Fabrication of Nano-Structured Ni-Al2O3 Graded Coatings: Structural Characterization. *Trans. Nonferrous Met. Soc. China* **2018**, *28*, 77–87. [CrossRef]
33. Winnicki, M.; Kozerski, S.; Malachowska, A.; Pawlowski, L.; Winnicki, M.; Kozerski, S.; Malachowska, A.; Pawlowski, L.; Optimization, M.R. Optimization of Ceramic Content in Nickel–Alumina Composite Coatings Obtained by Low Pressure Cold Spraying. *Surf. Coat. Technol.* **2021**, *405*, 126732. [CrossRef]
34. Feng, Q.; Li, T.; Teng, H.; Zhang, X.; Zhang, Y.; Liu, C.; Jin, J. Investigation on the Corrosion and Oxidation Resistance of Ni-Al_2O_3 Nano-Composite Coatings Prepared by Sediment Co-Deposition. *Surf. Coatings Technol.* **2008**, *202*, 4137–4144. [CrossRef]
35. Raghavendra, C.R.; Basavarajappa, S.; Sogalad, I. Multi-Objective Optimization of Electrodeposition of Ni–Al_2O_3Nano Composite Coating on Al6061 Substrate. *Trans. Indian Inst. Met.* **2018**, *71*, 2119–2132. [CrossRef]
36. Nagarajan, N.; Nicholson, P.S. Nickel-Alumina Functionally Graded Materials by Electrophoretic Deposition. *J. Am. Ceram. Soc.* **2004**, *87*, 2053–2057. [CrossRef]
37. Kumar, A.; Das, A.K. Fabrication of Al-Ni-Al2O3 Metal Matrix Composite Coating on AA1100 Wrought Aluminium Alloy by Gas Tungsten Arc (GTA) Coating Technique Fabrication of Al-Ni-Al2O3 Metal Matrix Composite Coating on AA1100 Wrought Aluminium Alloy by Gas Tungsten Arc. *Eng. Res. Express* **2022**, *4*, 035041. [CrossRef]
38. Pandiyarajan, S.; Manickaraj, S.S.M.; Liao, A.H.; Ramachandran, A.; Lee, K.Y.; Chuang, H.C. Recovery of Al_2O_3 from Hazardous Al Waste as a Reinforcement Particle for High-Performance Ni/Al2O3 Corrosion Resistance Coating via Ultrasonic-Aided Supercritical-CO2 Electrodeposition. *Chemosphere* **2023**, *313*, 137626. [CrossRef]
39. Sharma, A.; Biswas, P. The Utilization of Metal-Organic Frameworks (MOFs) Derived Nickel-Alumina Catalyst for the Production of Hydrogen-Rich Syn-Gas via Methane Tri-Reforming: An Innovative Approach for Attaining Enhanced Stability. *Int. J. Hydrogen Energy* **2024**, *77*, 1133–1146. [CrossRef]
40. Gheorghies, C.; Carac, G.; Stasi, I.V.; Dunarea, S.R.-G. Preparation and Structural Characterization of Nickel/Alumina Nano-Particles Composite Coatings. *J. Optoelectron. Adv. Mater.* **2006**, *8*, 1234–1237.
41. Sasi, A.; Mondal, M.; Dayal, S.; Kumar, S. Electro Deposition of Nickel-Alumina Composite Coating. *Mater. Today Proc.* **2015**, *2*, 3042–3048. [CrossRef]
42. Bensebaa, F.; Di Domenicantonio, D.; Scoles, L.; Kingston, D.; Mercier, P.; Marshall, G. Alternative Coating Technologies for Metal-Ceramic Nanocomposite Films: Potential Application for Solar Thermal Absorber. *Int. J. Low-Carbon Technol.* **2016**, *11*, 370–374. [CrossRef]
43. Lekka, M.; Lanzutti, A.; Casagrande, A.; de Leitenburg, C.; Bonora, P.L.; Fedrizzi, L. Room and High Temperature Wear Behaviour of Ni Matrix Micro- and Nano-SiC Composite Electrodeposits. *Surf. Coatings Technol.* **2012**, *206*, 3658–3665. [CrossRef]
44. Akhtar, K.; Khan, Z.U.; Gul, M.; Zubair, N.; Shah, S.S.A. Electrodeposition and Characterization of Ni-Al_2O_3Nanocomposite Coatings on Steel. *J. Mater. Eng. Perform.* **2018**, *27*, 2827–2837. [CrossRef]
45. Azizi-Nour, J.; Nasirpouri, F. Exploiting Magnetic Sediment Co-Electrodeposition Mechanism in Ni- Al_2O_3 Nanocomposite Coatings. *J. Electroanal. Chem.* **2022**, *907*, 116052. [CrossRef]

46. Irshad, H.M.; Hakeem, A.S.; Ahmed, B.A.; Ali, S.; Ali, S.; Ali, S.; Ehsan, M.A.; Laoui, T. Effect of Ni Content and Al_2O_3Particle Size on the Thermal and Mechanical Properties of Al2O3/Ni Composites Prepared by Spark Plasma Sintering. *Int. J. Refract. Met. Hard Mater.* **2018**, *76*, 25–32. [CrossRef]
47. Feng, Q.; Li, T.; Yue, H.; Qi, K.; Bai, F.; Jin, J. Preparation and Characterization of Nickel Nano-Al_2O_3 Composite Coatings by Sediment Co-Deposition. *Appl. Surf. Sci.* **2008**, *254*, 2262–2268. [CrossRef]
48. Huang, X.; Xiong, Y.; Liu, L.; Tian, Y.; Liu, G. Investigation on Nickel/Alumina-Nanoparticles Co-Deposition. *Microsyst. Technol.* **2009**, *15*, 723–729. [CrossRef]
49. Wazwaz, A.; Al-Salaymeh, A. Theoretical and Measured Optical Properties of Ni- Al_2O_3 over Al Substrate Selective Absorber. *Sustain. Cities Soc.* **2015**, *16*, 13–23. [CrossRef]
50. Galione, P.A.; Baroni, A.L.; Ramos-Barrado, J.R.; Leinen, D.; Martín, F.; Marotti, R.E.; Dalchiele, E.A. Origin of Solar Thermal Selectivity and Interference Effects in Nickel-Alumina Nanostructured Films. *Surf. Coatings Technol.* **2010**, *204*, 2197–2201. [CrossRef]